Biomolecule Interaction Analysis

DOI: 10.1002/anie.201402514

Thermophoresis in Nanoliter Droplets to Quantify Aptamer Binding**

*Susanne A. I. Seidel, Niklas A. Markwardt, Simon A. Lanzmich, and Dieter Braun**

Abstract: *Biomolecule interactions are central to pharmacology and diagnostics. These interactions can be quantified by thermophoresis, the directed molecule movement along a temperature gradient. It is sensitive to binding induced changes in size, charge, or conformation. Established capillary measurements require at least 0.5 μL per sample. We cut down sample consumption by a factor of 50, using 10 nL droplets produced with acoustic droplet robotics (Labcyte). Droplets were stabilized in an oil–surfactant mix and locally heated with an IR laser. Temperature increase, Marangoni flow, and concentration distribution were analyzed by fluorescence microscopy and numerical simulation. In 10 nL droplets, we quantified AMP-aptamer affinity, cooperativity, and buffer dependence. Miniaturization and the 1536-well plate format make the method high-throughput and automation friendly. This promotes innovative applications for diagnostic assays in human serum or label-free drug discovery screening.*

Molecular recognition is not only central to cell signaling, but it also represents the functional principle of pharmaceuticals and laboratory diagnostics. A variety of opportunities thus comes along with an in-depth understanding of biological binding events. From this perspective, it is not surprising to see an ever-growing interest in quantitative biomolecule interaction analysis. To this end, the directed movement of molecules along a temperature gradient, referred to as thermophoresis,[1] has been successfully utilized in the last years.[2,3] It is highly sensitive to molecular size, charge, and conformation. Based on binding induced changes in at least one of these parameters, affinity and concentration can be quantified, even in complex bioliquids.[4]

In the well-established microscale thermophoresis (MST) approach, samples are measured in glass capillaries. Capillary MST has been applied for ions, small molecules, nucleic acids, peptides, proteins, crude cell lysate, and untreated human blood serum.[4–6] With circa 0.5 μL per capillary filling, the sample consumption is low compared to, for example, isothermal titration calorimetry.[7] However, the actual measurement volume is significantly smaller: it lies in the range of 2 nL.[2] The additionally consumed volume becomes essential when working with expensive or rare material such as patient samples. This is especially true if high-throughput analyses need to be performed, for instance, in diagnostics or drug discovery. Throughput and automation of conventional MST are further limited by the complicated handling of glass capillaries.

Therefore, we developed a capillary-free approach to measure thermophoresis in nL droplets under an oil–surfactant layer inside 1536-well plates (Figure 1). The water-in-oil system was experimentally characterized for temperature induced effects. The findings agreed with numerical simulations.

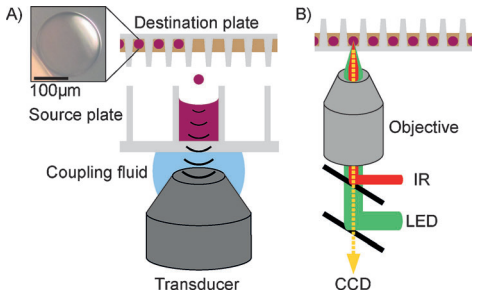

Figure 1. A) Droplet production. The liquid handler positions a destination plate above a source plate with a sample stock (purple). A transducer emits an acoustic pulse focused to the sample surface, whereby a 2.5 nL droplet travels into the destination well. To prevent evaporation, droplets are transferred into an oil–surfactant mix (brown). Inset: Samples were stable for several hours. 5 nL of 1:1 human serum/PBS. B) Inverted microscopic setup. The droplet center is heated with an IR laser. Thermophoresis is monitored by fluorescence (LED: light emitting diode; CCD: charge-coupled device camera).

The applicability of the system for biomolecule interaction studies was evaluated with a well-described nucleic acid aptamer. Aptamers were discovered more than 20 years ago.[8] Owing to their three-dimensional conformation, these single-stranded oligonucleotides bind to various biomedically relevant targets, including proteins and small molecules.[9,10] Just like antibodies, aptamers show high specificity and affinity. At the same time, these nucleic acid based ligands are superior to protein based ligands in production costs, storage conditions, and chemical modifiability.[10] In vivo, their small size facilitates good delivery to the target tissue,

[*] S. A. I. Seidel, N. A. Markwardt, S. A. Lanzmich, Prof. D. Braun
Systems Biophysics, Physics Department, NanoSystems Initiative Munich and Center for Nanoscience
Ludwig-Maximilians-University Munich
Amalienstrasse 54, 80799 Munich (Germany)
E-mail: dieter.braun@lmu.de
Homepage: http://www.biosystems.physik.lmu.de

[**] Financial support through a joint grant (BR2152/2-1) and project A4 within SFB 1032 from the Deutsche Forschungsgemeinschaft (DFG), by the Center for NanoScience (CeNS), and by the Nanosystems Initiative Munich (NIM) is gratefully acknowledged. The authors would like to thank Maximilian Weitz from the group of Friedrich C. Simmel for sharing his knowledge on microemulsions, Georg C. Urtel for support in building the setup and Christof B. Mast for programming support.

Supporting information for this article (including experimental details in Chapter 1) is available on the WWW under http://dx.doi.org/10.1002/anie.201402514.

whereas no immunogenicity and low toxicity have been reported.[10,11] These benefits and the first marketed aptamer drug demonstrate the high potential of aptamers.[12]

Aptamer binding studies were miniaturized employing a non-contact liquid handling system available commercially (Labcyte). The system delivers 2.5 nL portions from multi-well source plates into destination plates by acoustic droplet ejection (Figure 1 A).[13] The deviation from the target volume is less than 2% (Supporting Information, Chapter S3a). To prevent evaporation, droplets were transferred into a protective layer of standard microbiology mineral oil supplemented with a surfactant mix according to Tawfik and Griffiths.[14] For the presented experiments, we transferred four or eight 2.5 nL portions to yield 10 nL (270 μm) or 20 nL samples (340 μm). The positional accuracy of the transfer was reduced owing to deflection by the oil. To coalesce individual portions, destination plates with funnel-shaped wells were mildly centrifuged after transfer ($\leq$500 g to avoid droplet damage). With our optimized procedure, we reproducibly obtained nL samples that were stable for several hours (Figure 1 A, inset). This allowed for multiple thermophoretic binding assays (10 min each).

Droplets were measured on a newly constructed microscopic setup (Figure 1 B). Similar to the previously described capillary instrument,[2,5] thermophoresis was induced and analyzed all-optically. As an essential modification to the capillary setup, an inverted configuration was chosen so that the sample plate stayed upright to avoid oil dripping. While fixing the plate guaranteed that the droplets stayed in place, moving the optical parts allowed sequential measurements.

Before studying biomolecule affinity, we characterized the effects of local heating on aqueous nL droplets under oil. If asymmetrically applied, heating occasionally led to convective flows strong enough to move an entire droplet away from the laser spot. This was prevented by using plates with a small well floor area (r = 0.45 mm). Utilizing the temperature dependence of the fluorescent dye Alexa 647, the radial temperature profile in the central horizontal plane of a 20 nL droplet was obtained 0.2 s after the IR laser had been turned on (Figure 2 A). For a temperature increase of ΔT_c = 11 K in the heat spot center, the droplet periphery warmed up by ΔT_p = 4 K. A Lorentz fit revealed an FWHM of 120 μm. In the following, ΔT denotes the average temperature increase of the central (30 × 30) μm area.

Convective flows inside 20 nL samples were visualized with fluorescent polystyrene beads. Figure 2 B is integrated over 7 s of heating. The beads moved toward the central heat spot and out of focus, with peak velocities of 5–10 μm s^{-1} for ΔT = 6 K and 15 μm s^{-1} for ΔT = 15 K. To elucidate these flows, we performed full numerical simulations considering diffusion, convection, thermophoresis, and the temperature dependence of the dye. Simulations of 20 nL (Figure 3) and

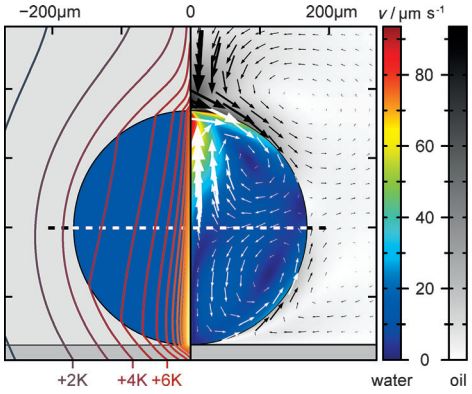

Figure 3. Numerical simulation of temperature and flow fields in a vertical cut through a 20 nL droplet after 0.2 s of heating. Left: Isotherms indicate the temperature increase. Right: The central horizontal plane (dashed) comprises the boundary of two toroidal flow vortices. The vortices are driven by Marangoni convection at the water–oil interface and have already reached the steady state.

10 nL droplets (Supporting Information, Figure S1) verified that the observed inward flow can be explained by Marangoni convection. This type of convection is caused by temperature-induced differences in interfacial tension. In our case, local heating decreased the interfacial tension between water and oil at the top and bottom of the droplet, triggering Marangoni fluid flow along the interface. Owing to the cylindrical symmetry, toroidal vortices arose in the upper and lower droplet hemisphere. Figure 3 shows the cross-sections of the tori in a vertical cut. The dashed line indicates the horizontal plane. Here, the flow is directed inward in the upper and lower vortex, which agrees with the experimental observation in this plane (Figure 2).

After flow field analysis, we recorded fluorescence time traces, the basis for our binding measurements, in 20 nL Alexa 647 samples (Figure 4 A). The experimental curves were highly reproducible and confirmed by simulation. A series of different events was identified in agreement with standard capillary measurements. When the heating laser was turned on, the fluorescence decreased owing to the temperature response (DTR) of the dye and thermophoretic molecule depletion. Thermophoresis and back-diffusion equilibrated within seconds. Subsequent slow warming of the entire sample slightly reduced the dye fluorescence intensity, but did not affect the measurement. When heating was turned off, fluorescence recovered owing to DTR and back-diffusion. A larger ΔT enhanced DTR and thermophoresis in experiment

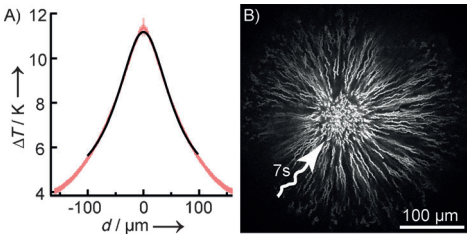

Figure 2. Local heating of 20 nL droplets. A) Radial temperature profile in the central horizontal plane (red). The temperature increased by ΔT_c = 11 K in the center and by ΔT_p = 4 K in the droplet periphery. A Lorentz fit (black) revealed FWHM = 120 μm. B) Flow profile of fluorescent polystyrene beads (d = 1.0 μm) integrated over 7 s during heating (ΔT = 15 K). The beads moved toward the heat spot and out of focus with a peak velocity of 15 μm s^{-1}.

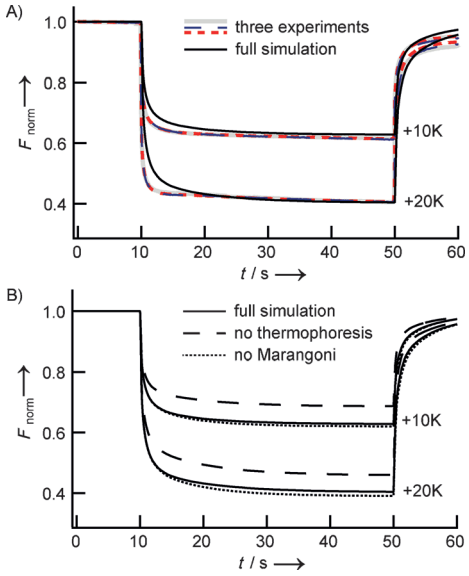

Figure 4. Fluorescence time traces from 20 nL droplets. A) Measurements of three Alexa 647 samples (gray, blue, red) overlap with minor deviations demonstrating the low batch-to-batch variation. Experiments and simulation (black) agree well. After the IR laser is turned on ($t = 10$ s), the fluorescence decreases due to the temperature response (DTR) of the dye and thermophoresis. Thermophoresis and back-diffusion equilibrate within seconds. After heating ($t = 50$ s), F_{norm} recovers due to DTR and isothermal back-diffusion. A larger ΔT enhances DTR and thermophoresis. B) Simulated contributions to the decrease in F_{norm}. Omitting Marangoni convection led to a negligible change of 0.008 (dotted); omitting thermophoresis changed the signal by 0.06 (dashed).

and simulation (Figure 4A). To assess the contribution of Marangoni convection and thermophoresis, simulations excluding either effect were performed (Figure 4B; implementation details are given in the Supporting Information, Chapter S2a). When neglecting Marangoni convection, the flow fields differed considerably, but the fluorescence signal was only slightly altered. Upon removal of thermophoresis from the simulation, the time traces changed significantly. This demonstrates that thermophoresis prevailed against the convective flows.

Having characterized thermophoresis in nL droplets under oil, we evaluated its applicability for biomolecule interaction studies. We analyzed a 25 mer DNA aptamer that binds adenosine and its phosphorylated analogues.[15] This aptamer has previously been studied extensively.[2,16] For nL-scale interaction studies, a constant concentration of fluorescently labeled aptamer ($c = 2$ μM) was added to a serial dilution of adenosine-5′-monophosphate (AMP). As mentioned above, mild centrifugation in the funnel-shaped wells reliably coalesced individual AMP and aptamer portions. After coalescence, the concentration of AMP and aptamer equilibrated by diffusion. The short diffusion times through the small 10 nL or 20 nL samples guaranteed complete mixing within minutes. We found diffusive mixing to be as effective as manual premixing.

The mixed samples were locally heated by $\Delta T = 6$ K. The resultant thermophoretic depletion of free aptamer significantly differed from its bound complex with AMP (Supporting Information, Figure S2). Furthermore, the temperature response of the aptamer dye (DTR) changed upon AMP binding.

The fluorescence after DTR and thermophoresis was divided by the fluorescence before heating as described in the Supporting Information, Figure S2 and previously.[6] As this relative fluorescence can be approximated as linear to the bound aptamer fraction, it was directly fit to the Hill equation (Supporting Information, Chapter S3c).

Using the original selection buffer according to Huizenga and Szostak,[15] we found $EC_{50} = (116 \pm 14)$ μM in 10 nL samples and $EC_{50} = (104 \pm 10)$ μM in 20 nL samples (Figure 5A). Both values agree with each other and the literature value of (87 ± 5) μM from capillary thermophoresis.[2] The determined Hill coefficients of $n = 1.2 \pm 0.1$ (10 nL) and $n = 1.9 \pm 0.3$ (20 nL) indicate cooperative binding of more than one AMP, which is consistent with the previously reported tertiary structure of the complex (Figure 5, inset).[17] Moreover, the Hill coefficients only slightly deviate from each other and confirm the literature value ($n = 1.4$).[2] As a control, we measured a DNA oligonucleotide with the same length as the aptamer but two point mutations. The dinucleotide

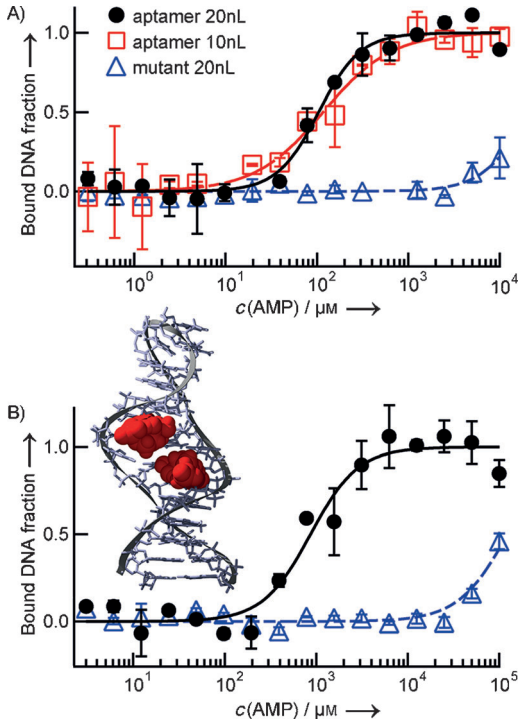

Figure 5. The specific signal change in DTR and thermophoresis upon AMP titration to labeled aptamer was fit to the Hill equation. Mean values of at least two individual nL samples; error bars: standard deviation. A) Selection buffer. The fit revealed $EC_{50} = (116 \pm 14)$ μM and $n = 1.9 \pm 0.3$ in 10 nL (red squares) and $EC_{50} = (104 \pm 10)$ μM and $n = 1.2 \pm 0.1$ in 20 nL (black circles). A dinucleotide mutant showed a 200-fold increased EC_{50} value of about 20 mM (blue triangles). (B) PBS. $EC_{50} = (0.90 \pm 0.13)$ mM was found (black circles), confirming the buffer dependence of the aptamer ($n = 1.6 \pm 0.4$). The mutant showed a 130-fold increased EC_{50} value of about 0.12 M (blue triangles). Inset: Determined Hill coefficients agree with the reported tertiary structure (NDB code 1AW4): an aptamer (gray) binds two AMP molecules (red).[17]

mutant showed a 200-fold reduced AMP-affinity ($EC_{50} \approx 20$ mM). This demonstrates the specificity of the binding signal.

To quantify the reported buffer dependence of the AMP-aptamer,[2] binding was measured in PBS (Figure 5B). An EC_{50} of (0.90 ± 0.13) mM was found, corresponding to a 10-fold affinity reduction compared to selection buffer. This reduction is not surprising, as the aptamer has originally been evolved in and thus optimized for its selection buffer.[15,18] A dominant effect can most likely be ascribed to magnesium ions: while the selection buffer contained 5 mM $MgCl_2$, we used PBS without Mg^{2+}. Mg^{2+} do not only stabilize DNA, but can also neutralize AMP phosphate group and thus reduce repulsion to phosphates in the aptamer backbone.[19] A reduction of the $MgCl_2$ concentration from 5 to 0 mM has been reported to significantly reduce AMP-aptamer retention in affinity chromatography.[16] This is in accordance with the EC_{50} differences that we found in nL-thermophoresis. The Hill coefficient was not significantly affected by the buffer; it was $n = 1.6 \pm 0.4$ in PBS. The affinity of the mutant control was reduced 130-fold compared to the aptamer ($EC_{50} \approx 0.12$ M).

The successful quantification of affinity, cooperativity, and buffer dependence confirms the applicability of the presented method for aptamer analysis. This type of study is most likely to gain in importance now that the comprehensive aptamer patent portfolio, which presumably has suppressed many commercial applications, is starting to expire.[20] Furthermore, nL-thermophoresis is a highly attractive analytical method for other biomolecules including peptides or proteins, and for complex bioliquids such as blood. The suitability for these studies remains to be tested, but can be expected judging from the application depth of capillary thermophoresis.[4–6] Sample preparation is unlikely to be limiting, as the liquid handler can be deployed for various solution types. We, for example, produced stable nL droplets of 50% human blood serum (Figure 1A, inset) as required for thermophoretic diagnostics. Diffusive mixing after nL transfer was successful. Therefore, an assay design in which a stock dilution series of a biomolecule target is tested against a high number of binding partners seems very practical, for example, for drug discovery. It could also be combined with our previously published diagnostic autocompetition approach.[4] A stock dilution of an unlabeled tracer for the biomarker of interest would then be tested against multiple patient sera, supplemented with a constant amount of labeled tracer.

Compared to conventional capillary thermophoresis, the volume was reduced 50-fold. This leads to an enormous potential for high-throughput screens, even more so, as the easy-to-handle multi-well plates promote automation.

As a further advantage, the nL transfer is contact-free, which exempts from washing steps and minimizes cross-contaminations. After transfer, the sample is not in direct contact with the well surface, but forms a surfactant surrounded droplet inside the oil. This should significantly reduce unspecific surface adhesion of biomolecules ("sticking"), an often encountered challenge in capillary thermophoresis.[6] The elimination of sticking represents a major benefit, even if surfactant and oil might have to be optimized for different sample types.

Considering these advantages, the miniaturization, and the extensive characterization in experiment and simulation, nL droplet thermophoresis promises diverse applications throughout the life sciences.

Received: February 17, 2014
Revised: April 11, 2014
Published online: June 4, 2014

Keywords: analytical methods · binding affinity · high-throughput screening · nanoliter thermophoresis · numerical simulation

[1] a) C. Ludwig, *Sitzungsber. Akad. Wiss. Wien Math.-Naturwiss. Kl.* **1856**, 539; b) S. Duhr, D. Braun, *Proc. Natl. Acad. Sci. USA* **2006**, *103*, 19678 – 19682.
[2] P. Baaske, C. J. Wienken, P. Reineck, S. Duhr, D. Braun, *Angew. Chem.* **2010**, *122*, 2286 – 2290; *Angew. Chem. Int. Ed.* **2010**, *49*, 2238 – 2241.
[3] a) C. J. Wienken, P. Baaske, U. Rothbauer, D. Braun, S. Duhr, *Nat. Commun.* **2010**, *1*, 100; b) L. C. Hinkofer, S. A. I. Seidel, B. Korkmaz, F. Silva, A. M. Hummel, D. Braun, D. E. Jenne, U. Specks, *J. Biol. Chem.* **2013**, *288*, 26635 – 26648.
[4] S. Lippok, S. A. I. Seidel, S. Duhr, K. Uhland, H.-P. Holthoff, D. Jenne, D. Braun, *Anal. Chem.* **2012**, *84*, 3523 – 3530.
[5] S. A. I. Seidel, C. J. Wienken, S. Geissler, M. Jerabek-Willemsen, S. Duhr, A. Reiter, D. Trauner, D. Braun, P. Baaske, *Angew. Chem.* **2012**, *124*, 10810 – 10814; *Angew. Chem. Int. Ed.* **2012**, *51*, 10656 – 10659.
[6] S. A. I. Seidel, P. M. Dijkman, W. A. Lea, G. van den Bogaart, M. Jerabek-Willemsen, A. Lazic, J. S. Joseph, P. Srinivasan, P. Baaske, A. Simeonov, I. Katritch, F. A. Melo, J. E. Ladbury, G. Schreiber, A. Watts, D. Braun, S. Duhr, *Methods* **2013**, *59*, 301 – 315.
[7] T. Wiseman, S. Williston, J. F. Brandts, L.-N. Lin, *Anal. Biochem.* **1989**, *179*, 131 – 137.
[8] a) C. Tuerk, L. Gold, *Science* **1990**, *249*, 505 – 510; b) A. D. Ellington, J. W. Szostak, *Nature* **1990**, *346*, 818 – 822.
[9] A. D. Keefe, S. Pai, A. Ellington, *Nat. Rev. Drug Discovery* **2010**, *9*, 537 – 550.
[10] A. Wochner, M. Menger, M. Rimmele, *Expert Opin. Drug Discovery* **2007**, *2*, 1205 – 1224.
[11] R. S. Apte, M. Modi, H. Masonson, M. Patel, L. Whitfield, A. P. Adamis, *Ophthalmology* **2007**, *114*, 1702 – 1712.
[12] E. S. Gragoudas, A. P. Adamis, E. T. Cunningham, M. Feinsod, D. R. Guyer, *N. Engl. J. Med.* **2004**, *351*, 2805 – 2816.
[13] R. Ellson, M. Mutz, B. Browning, L. Lee, Jr., M. Miller, R. Papen, *JALA* **2003**, *8*, 29 – 34.
[14] D. S. Tawfik, A. D. Griffiths, *Nat. Biotechnol.* **1998**, *16*, 652 – 656.
[15] D. E. Huizenga, J. W. Szostak, *Biochemistry* **1995**, *34*, 656 – 665.
[16] Q. Deng, I. German, D. Buchanan, R. T. Kennedy, *Anal. Chem.* **2001**, *73*, 5415 – 5421.
[17] C. H. Lin, D. J. Patel, *Chem. Biol.* **1997**, *4*, 817 – 832.
[18] E. J. Cho, J.-W. Lee, A. D. Ellington, *Annu. Rev. Anal. Chem.* **2009**, *2*, 241 – 264.
[19] H. Sigel, *Chem. Soc. Rev.* **1993**, *22*, 255 – 267.
[20] P. Dua, S. Kim, D.-K. Lee, *Recent Pat. DNA Gene Sequences* **2008**, *2*, 172 – 186.

